Non-Contact Assessment of Peripheral Artery Haemodynamics Using Infrared Video Thermography

João Jorge, Mirae Harford, Mauricio Villarroel, Sitthichok Chaichulee, Shaun Davidson, Eoin Finnegan, Samuel H. Clark, J. Duncan Young, Peter J. Watkinson, and Lionel Tarassenko

***Abstract*—Skin temperature has long been used as a natural indicator of vascular diseases in the extremities. Considerable correlation between oscillations in skin surface temperature and oscillations of skin blood flow has previously been demonstrated. We hypothesised that the impairment of blood flow in stenotic (subcutaneous) peripheral arteries would influence cutaneous temperature such that, by measuring gradients in the temperature distribution over skin surfaces, one may be able to diagnose or quantify the progression of vascular conditions in whose pathogenesis a reduction in subcutaneous blood perfusion plays a critical role (*e.g.* peripheral artery disease). As proof of principle, this study investigates the local changes in the skin temperature of healthy humans (15 male, 30.0 $\pm$ 5.2 years old, BMI 25.1 $\pm$ 2.2 kg/m^2) undergoing two physical challenges designed to vary their haemodynamic status. Skin temperature was measured in four central regions (forehead, neck, chest, and left shoulder) and four peripheral regions (left upper arm, forearm, wrist, and hand) using an infrared thermal camera. We compare inter-region patterns. Median temperature over the peripheral regions decreased from baseline after both challenges (maximum decrease: -2.09 ± 0.41 °C at 60 s after exercise; $p = 0.0001$ and -0.58 ± 0.14 °C at 180 s of cold-water immersion; $p = 0.0013$). Median temperature over the central regions showed no significant changes. Our results show that the non-contact measurement of perfusion-related changes in peripheral temperature from infrared video data is feasible. Further research will be directed towards the thermographic study of patients with symptomatic peripheral vascular disease.**

***Index Terms*—Exercise physiology, blood flow imaging, perfusion, infrared thermography, temperature regulation during exercise, reactions to cold, skin temperature, non-invasive imaging.**

I. Introduction

PERIPHERAL arterial disease (PAD) of the lower extremities is a highly prevalent condition. It is estimated to affect between 4.5% and 29% of the population worldwide and more than 20% of those over 75 years of age [1]. PAD significantly impairs functional capacity and quality of life and is an early indicator of future cardiovascular and cerebrovascular events; some 60% of patients with PAD will have ischaemic heart disease, and 30% have cerebrovascular disease [2]. Diabetes mellitus and smoking are the main risk factors for symptomatic PAD [3]. Other risk factors include old age, male gender, dyslipidemia, hypertension, hyperhomocyteinemia, and renal insufficiency [4].

PAD designates a range of arterial syndromes that are caused by atherosclerotic obstruction of arteries in the lower extremities [5]. As plaque builds up in the arteries carrying blood from the heart to the peripheries, the extent of plaque increase leads to narrowing of the lumen, thus restricting blood flow (BF) to the periphery, and reducing the ability of the body to regulate the peripheral temperature [6]. We hypothesise that an abnormal distribution of surface temperature over the extremities may, therefore, be an indicator of abnormal blood flow supply to the affected regions.

Peripheral BF can be considered as a source of longitudinal thermal waves propagating from the subcutaneous vessel network towards the skin surface. The velocity of propagation and amplitude attenuation of the thermal wave depend on the medium through which it propagates (*i.e.* the skin). According to heat transfer theory, cutaneous temperature (T_c) is influenced by various factors, including local blood perfusion, heat conduction from deeper tissues (including muscle) and heat loss along the skin's surface (*e.g.* due to the thickness of subcutaneous fat and subcutaneous tissue blood perfusion [7], [8]). Among these

Manuscript received January 9, 2020; revised March 24, 2020 and May 18, 2020; accepted May 27, 2020. Date of publication June 5, 2020; date of current version December 21, 2020. This work was supported in part by the RCUK Digital Economy Programme, under Grant EP/G036861/1 (Oxford Centre for Doctoral Training in Healthcare Innovation), in part by the Fundacao para a Ciencia e Tecnologia, Portugal, doctoral under Grant SFRH/BD/85158/2012, in part by the National Science and Technology Development Agency, Thailand and in part by the NIHR Oxford Biomedical Research Centre. *(Corresponding author: Joao Jorge.)*

João Jorge is with the Department of Engineering Science, Institute of Biomedical Engineering, University of Oxford, Oxford OX1 2JD, U.K. (e-mail: joao.jorge@eng.ox.ac.uk).

Mirae Harford, J. Duncan Young, and Peter J. Watkinson are with the Nuffield Department of Clinical Neurosciences, Kadoorie Centre for Critical Care Research and Education, University of Oxford.

Mauricio Villarroel, Sitthichok Chaichulee, Shaun Davidson, Eoin Finnegan, and Lionel Tarassenko are with the Department of Engineering Science, Institute of Biomedical Engineering, University of Oxford.

Samuel H. Clark is with the Department of University College London Hospital Critical Care, University College London Hospitals NHS Foundation Trust.

This article has supplementary downloadable material available at http://ieeexplore.ieee.org, provided by the authors.

Digital Object Identifier 10.1109/TBME.2020.2999539

factors, blood perfusion is the dominant factor [9], and thus local fluctuations in T_c are largely dependent on oscillations in the supply of subcutaneous BF.

The fluctuations of BF in peripheral vessels are well documented [10]. The spectral dependence of T_c oscillations in the periphery upon oscillations in BF to peripheral vessels is associated with several physiological processes; five frequency bands have been identified corresponding to endothelial ([0.005–0.02] Hz), neurogenic ([0.02–0.05] Hz), myogenic ([0.05–0.15] Hz), respiratory ([0.15–0.4] Hz), and cardiac ([0.4–2.0] Hz) activity [11]. The delay time and amplitude attenuation in T_c oscillations in relation to BF oscillations (*i.e.* their frequency response) have been determined in the endothelial and the neurogenic frequency bands using wavelet spectral analysis [12]. In this seminal work, the authors established the interrelation between the dynamics of BF and skin temperature in the frequency domain, thus establishing the possibilities and the limitations on the use of temperature measurements as a method for BF assessment in the extremities.

Human skin, with an emissivity value of 0.98 [13], is a particularly suitable material for temperature measurement using thermal imaging [14]. Infrared thermal imaging can measure superficial skin temperature through the measurement of the spontaneous thermal irradiation of the human body. Thermographic imaging is accomplished with a camera that converts infrared radiation (IR) into a visual image that depicts temperature variations across an object or scene. Since it first became available for non-military applications in 1958 [15], IR technology has become economically more viable, technically more reliable and considerably more portable. The miniaturisation of IR detectors has rendered IR technology ubiquitous, with manufacturers even producing affordable mobile thermal cameras [16]. Within recent years some progress has also been made in improving standardization protocols for quantitative thermography [17]. These advancements have led to an increase in the use of thermal imaging in medical and clinical applications [18]–[20]. IR thermography has been used to study a number of diseases where skin temperature can reflect the presence of inflammation in underlying tissues (*e.g.* inflammatory arthritis [21], osteoarthritis [22]–[24], and soft tissue rheumatism [25]–[27]), pain syndromes [28]–[30], immune response (*e.g.* fever screening [31]), or abnormal BF due to a clinical abnormality (*e.g.* as a result of Raynaud's phenomenon [32], [33], diabetic foot [34] or malignant diseases [35]–[37]).

Several advances in the thermographic imaging of blood perfusion have been made in recent decades. In 1979, Francis *et al.* proposed a method for measuring skin surface blood perfusion through the distribution of regional variations in body surface temperature via IR thermal imaging [38]. Using IR thermal imaging, Pavlidis *et al.* monitored changes in blood perfusion on the body surface [39], [40]. Active approaches have also been attempted. Using a Peltier heating element to provide external thermal stimulation, Boue *et al.* developed a thermographic method to estimate the radius, depth and BF velocity in a vein of the forearm based on a model of heat diffusion [41]. Jin *et al.* proposed a method for measuring BF velocity in superficial arteries using (laser-induced) dynamic IR thermal imaging [42].

As most PAD patients with early vascular disease are asymptomatic, patients require aggressive control of modifiable risk factors. Several techniques are currently used to screen lower extremity PAD. These include ankle-brachial pressure index (ABPI), segmental limb pressure, toe pressure, and ultrasound [43]. Angiographic approaches - based on either CT or MR imaging - are usually used for diagnosis confirmation, severity assessment, anatomical evaluation, and treatment planning [43]. By detecting perfusion-related changes in T_c, infrared thermography could provide a contrast agent-free alternative to the assessment of blood perfusion in the periphery [44]. Such a system would have several advantages over conventional tools for the functional assessment of vascular health or the screening of diseases in the extremities, such as PAD. IR thermography is convenient, and non-invasive, which is guaranteed by the absence of contact devices or contrast agents. Additionally, modern thermal IR imaging devices are portable, affordable, and can record body temperature changes over time. By leveraging the relationship between the haemo- and the thermo-dynamics of skin perfusion, these devices could prove to be reliable monitors for the non-invasive testing of the functional effect of PAD.

The purpose of this study was to characterise the skin thermal response to changes in peripheral perfusion. Two physical challenges were designed to induce changes in the peripheral perfusion in healthy young volunteers through changes in their peripheral vascular tone. Central and peripheral haemodynamics were assessed during incremental leg exercise in the upright position (exercise stimulus) and a cold pressor test (cold stimulus). We hypothesised that (1) both stimuli would lead to a decrease in peripheral perfusion to the non-exercising/non-immersed upper limbs, and (2) that the perfusion-related changes in the distribution of T_c over non-exercising/non-immersed areas could be detected non-invasively using IR thermography.

II. Methods

Both hypotheses were tested using thermal video recordings of healthy volunteers who underwent two physical challenges designed to vary their cardiac output/peripheral blood flow in a controlled manner and under controlled illumination. The study group consisted of 15 young healthy male volunteers. All subjects were double-monitored, with both challenges carried out under concurrent video and vital-sign monitoring. A description of the study protocol, monitoring equipment and protocols for data acquisition and analysis is given below.

A. Subjects

Fifteen healthy volunteers of eligible age (18–60 years) were recruited. Male subjects were recruited to facilitate simultaneous image recording from multiple regions of exposed skin. Exclusion criteria were: Participants whose anatomy, condition, or other required monitoring precluded the use of camera equipment, transthoracic echocardiogram, or thoracic bioimpedance measurement (*e.g.* thoracic wall deformity not allowing transthoracic echocardiography), history of cardiovascular disease, or any current or previous leg injuries which precluded the use of a bicycle-like device.

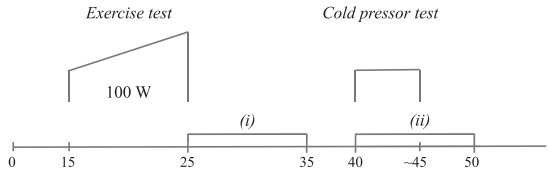

Fig. 1. Schematic of the experimental protocol illustrating the baseline period ([0; 15] min), the exercise test ([15; 25] min), the first period of interest ([25; 35] min), the cold pressor test (until pain), and the second period of interest (10 min after the start of CPT). Thermographic and physiological recording was continuous from $t = 0$ to the end of the experimental period.

B. Study Design

The study was conducted in the Kadoorie Centre for Critical Care Research and Education, John Radcliffe Hospital, Oxford, United Kingdom. It was carried out in accordance with the Declaration of Helsinki and approved by the Oxford University Research and Ethics Committee/Clinical Trials and Research Governance (R45629/RE003) and Oxford University Hospitals NHS Foundation Trust ethics board (R&D reference:12056). Written informed consent was obtained from all participants.

Measurements were carried out in optimal conditions (seated position, room temperature). According to International Academy of Clinical Thermology (IACT) guidelines [45], prior to the haemodynamic challenges, baseline radiometric images were obtained with the participant at rest for a 15-min period (baseline). This period was useful both for thermal acclimatisation to the experimental room and stabilisation of the physiological status of the participants. After this period, the protocol described below and shown in Fig. 1 was adopted. Each participant performed an exercise test (ET) under constant workload for 10 minutes using a pedal exerciser at a set resistance (equivalent to 100 W at 60 rotations per minute). The exercise regimen was approved by a physiotherapy team and the equipment was checked to ensure the safety of the participants. After a 15-min recovery period, the participant immersed their right hand in ice water at a temperature of 4 °C to a point just above the wrist for five minutes or until the point of pain (as reported by each participant), following the original description of the cold pressor test (CPT) in Hines *et al.* [46]. Recording continued during a second recovery period of 10 minutes after the end of this test. In total, each recording session lasted between 50 and 55 minutes. Thermographic and physiological recording was continuous throughout the experimental period. Echocardiography was performed at 1-min intervals prior to ET and after this intervention.

We defined two periods of interest as (i) the 10 minutes immediately following the cessation of ET, and (ii) the 10 minutes following the start of the CPT.

C. Instrumentation

Room illumination was delivered by two 5600 K LED mosaic panels (576 diodes over a $30 \times 30\,\text{cm}^2$ area), each held by a stand approximately 2 m away from the subject and set at a height of 1.6 m. Ambient room temperature (±0.8 °C) and relative humidity (±4%) were monitored using an hygro-thermometer (Extech SD500, Extech Instruments, Nashua, New Hampshire, USA) placed on a table next to the participant.

All thermal images were acquired using a MWIR thermal imaging camera (FLIR Instruments A6703, Oregon, USA) operating in the spectral range of 3–5 μm with a temperature sensitivity <20 mK. The camera was positioned 1.5 m away from the seated participant using a tripod (244RC, Manfrotto, Cassola, Italy) perpendicular to the plane of the chest of the participant to be imaged. The imaging device was set to acquire 16-bit radiance images at a rate of 60 frames per second and at a spatial resolution of 512×640 pixels.

To monitor the cardiovascular status, two non-invasive methods were used. A chest impedance monitor (CardioScreen 1000, Medis, Ilmenau, Germany) was used to obtain beat-to-beat estimates of stroke volume (SV) by thoracic electrical bioimpedance (TEB). The device was attached to the torso of the participant using adhesive sensors applied to the skin on both sides of the neck and lower chest at the level of the diaphragm. An arterial compliance modulation (ACM) sensor was used to measure arterial pulse waves via earlobe photoplethysmography (PPG). Additionally, a qualified cardiac sonographer acquired transthoracic echocardiogram (TTE) video sequences at one-minute intervals using an ultrasound system (Philips CX50-US, Philips Ultrasound Systems, Eindhoven, Netherlands). TTE was performed before the experiment (to measure aortic root diameter and the velocity time integral) and then at 1-min intervals for ten minutes after each intervention. TTE was not acquired during ET as images of good echographic quality are not possible due to participant movement. Two blinded cardiac sonographers performed SV measurements from the TTE images offline. The mean of the two measurements was used for each image. Previous work by Harford *et al.*, established a good agreement between SV changes detected by TTE and TEB in this dataset, with TEB being able to detect significant changes in SV [47]. Thus, given the equivalence between the two techniques and the higher sampling rate afforded by TEB (1 Hz versus 1/60 Hz in TTE), in this study we report estimates of SV measured by TEB. Blood pressure (BP) was measured at one-minute intervals using a brachial cuff applied to the right arm (M10-IT oscillometric monitor, Omron Healthcare, Ltd., Kyoto, Japan).

Additionally, an optical sensor (Masimo M-LNCS DBI, Masimo, Irvine, USA) was applied to the left index finger to acquire the PPG signal at 256 Hz. Continuous 1-lead bipolar ECG signals were collected and digitised at 256 Hz. All ancillary signals were recorded by a Visi BlackShadow system (Stowood Scientific Instruments, Oxford, UK), which provided estimates of the cardiorespiratory vital signs (HR and RR) at a rate of at 1 Hz. Estimates of cardiac output (CO) were calculated as the product between SV and HR values. Estimates of total peripheral resistance (TPR) were obtained as the ratio between mean arterial pressure (MAP) and CO.

D. Data Analysis

We propose a novel method for the analysis of radiance images for the non-contact measurement of perfusion-related

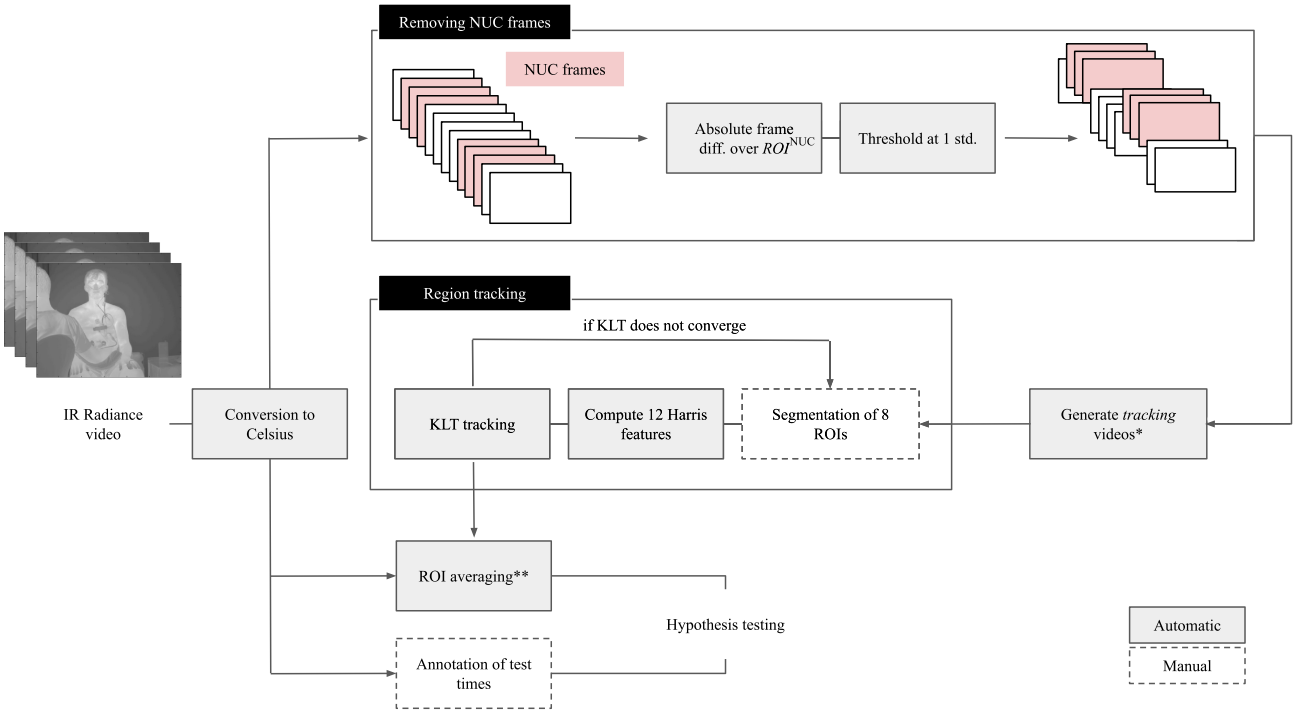

Fig. 2. Overview of the protocol for data analysis. After the pixel-wise conversion of the radiance measured to temperature values, frames acquired during Non-Uniform Correction (NUC) are removed. Thermal areas of interest are detected and then tracked using the Kanade-Lucas-Tomasi (KLT) algorithm. Manual operations are shown in white blocks, while automatic operations are shows in grey-shaded blocks. * using 1/10 frame rate decimation, large motion elimination, and image compression. ** pixel average computed over the one third of pixels with highest intensity within each region-of-interest (ROI). See main text for further details.

changes in skin temperature from infrared video data, as shown schematically in the diagram of Fig. 2 and described in the sections below. This method takes as single input the radiance images and produces the time series T_c over the thermal areas of interest.

1) Conversion From IR Radiance to Celsius: Each radiance image was converted into a temperature map by computing the temperature value corresponding to each pixel from the total radiation received by that sensor element, in W/m^2. The total radiation received by a camera sensor (W_{total}), originates from three sources: the emission of the target object (E_{obj}), the emission of the surroundings and reflected by the object (E_{ref}) and the emission of the atmosphere (E_{atm}). It can be expressed as Equation 1 [48].

$$W_{total} = E_{obj} + E_{ref} + E_{atm} \tag{1}$$

The first source is the emission from the target object. However, not all radiation emitted by the target object is received by the thermal camera; some is absorbed by the atmosphere as a function of the transmittance of this medium (τ_{atm}). Thus, according to Stefan-Boltzmann's law, the emission of the target object takes the form of Equation 2.

$$E_{obj} = \epsilon_{obj}\, \tau_{atm}\, \sigma (T_{obj})^4 \tag{2}$$

where ϵ_{obj} is the emissivity of the object, T_{obj} is temperature of the object, and σ is the Stefan-Bolzmann's constant (5.67×10^8 W/m^{2}K^4).

As thermography operates only inside limited spectral ranges, it is common practice to treat target objects as grey bodies. Grey bodies have a reflectivity greater than zero. Thus, they reflect the infrared radiation emitted by the surroundings. Part of this reflected radiation is also absorbed by the atmosphere. This is the second component received by the camera (E_{ref}) and can be expressed as Equation 3.

$$E_{ref} = \rho_{obj}\, \tau_{atm}\, \sigma (T_{ref})^4) = (1 - \epsilon_{obj})\, \tau_{atm}\, \sigma\, (T_{ref})^4 \tag{3}$$

where ρ_{obj} is the spectral reflectance of the object, and T_{ref} is the reflected ambient (background) temperature. It is an effective value, as it is normally assumed that T_{ref} is the same for all emitting surfaces within the half-sphere seen from a point on the object's surface. The third component is the emission of infrared radiation from the atmosphere. This component can be expressed as Equation 4, where $(1 - \tau_{atm})$ is the emittance of the atmosphere and temperature of the atmosphere (T_{atm}).

$$E_{atm} = \epsilon_{atm}\, \sigma\, (T_{atm})^4 = (1 - \tau_{atm})\, \sigma\, (T_{atm})^4 \tag{4}$$

Finally, using Equation 1 to combine Equations 2, 3, and 4, we obtain the relation we seek between the temperature of the target object T_{obj} and the total radiation received by the camera sensor W_{total} in Equation 5.

$$T_{obj} = \sqrt[4]{\frac{W_{total} - E_{ref} - E_{atm}}{\epsilon_{obj}\, \tau_{atm}\, \sigma}} \tag{5}$$

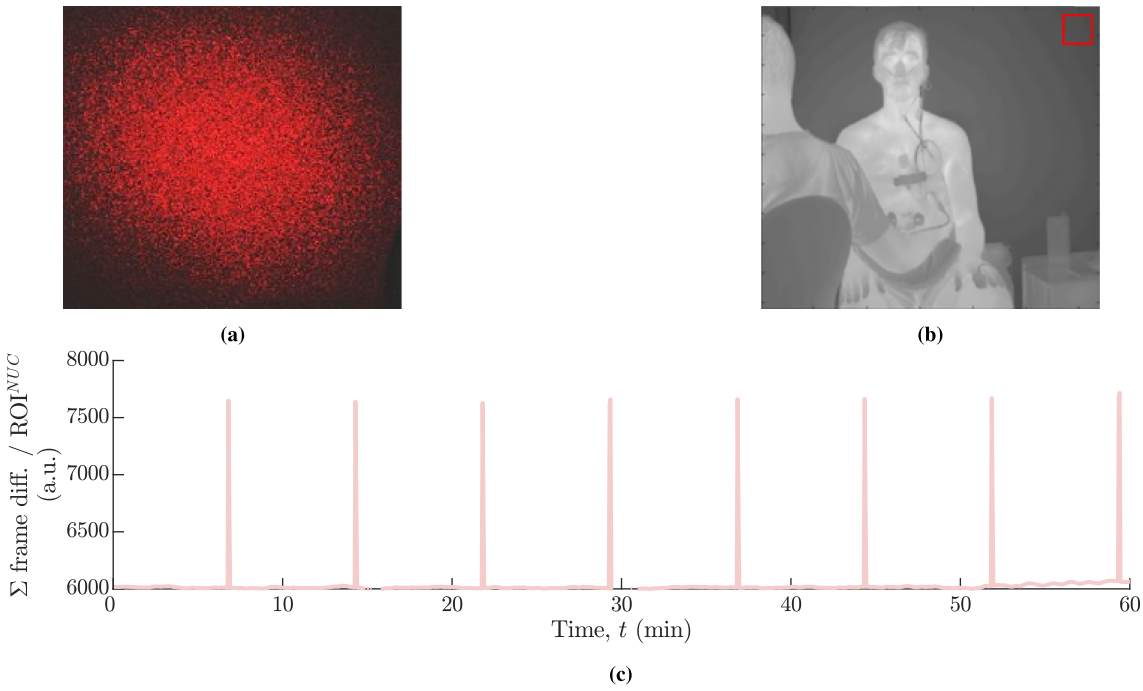

Fig. 3. Protocol for the detection of NUC frames. (a) Sample NUC frame. (b) Sample radiance image. The 15 × 15 pixel ROI^{NUC} is shown as a red box in the top-right corner of the frame. (c) Sum of pixel-wise frame differences computed over ROI^{NUC} between consecutive frames for a sample study session. NUC frames were identified as the frames for which $\mu_{ROI^{NUC}}(t)$ was above 2 standard deviations of its median value for all study sessions.

In order to solve Equation 5 the emissivity of the object (ϵ_{obj}), the reflected temperature (T_{ref}), the transmittance of the atmosphere (τ_{atm}) and the temperature of the atmosphere (T_{atm}) must be supplied. τ_{atm} was estimated using the distance from the object to the camera (1.5 m) and the relative humidity trace obtained using the room hygro-thermometer. In general, this value was very close to one. T_{atm} was similarly obtained using the room hygro-thermometer. In practice, as $(1 - \tau_{atm})$ is very close to zero, T_{atm} has little influence on the temperature measurement. In contrast, accurate measurement of ϵ_{obj} and the reflected temperature are particularly important, as these exert great influence on the temperature measurement. The emissivity describes how much energy is emitted as thermal energy from the target object at a given object temperature compared to that from a black body at the same temperature. Therefore, low-emissivity materials emit less infrared radiation than materials with high emissivity at the same temperature. Steketee *et al.*, established that the emissivity of skin tissue is nearly constant [13]. Therefore, a constant emissivity of 0.98 was used.

2) Non-Uniformity Compensation: A fundamental difference between thermal IR cameras and visible light cameras, whose sensors are mostly complementary metal–oxide–semiconductor (CMOS) devices, lies in the fact that IR sensors are thermo-sensitive. As such, their response can vary as a function of ambient temperature, and therefore, the pixels in thermal cameras may not respond identically with respect to neighbouring pixels. To mitigate this effect, thermal cameras perform Non-Uniformity Compensation (NUC), a necessary calibration process used to normalize their pixel-to-pixel output. In our recordings, this process occurs every 10 minutes and lasts for approximately 5 seconds per calibration. We designed a simple algorithm to identify the indices of frames collected during this calibration process (NUC frames) and exclude them from further analysis. To achieve this, we computed the average pixel intensity $\mu_{ROI^{NUC}}(t)$ over the 15 × 15 pixel area on the top-right corner of the frame (ROI^{NUC}). This quantity was computed for every frame captured. NUC frames were identified as the frames for which $\mu_{ROI^{NUC}}(t)$ was above 2 standard deviations of its median value over all study sessions. This process is illustrated in Fig. 3.

3) Tracking Thermal Areas: We manually identified 8 regions-of-interest (ROIs) in the first frame of each session: the forehead, the neck, the upper thorax, and the left axilar region (*i.e.* the core regions), the anterior views of the left shoulder, the left upper arm, the left wrist, and left hand (*i.e.* the peripheral regions). This process is illustrated in Fig. 4 for a sample frame. The left lateral structures were selected to avoid ROI occlusion during the TTE measurements or CPT.

The position and shape of the ROIs were tracked on subsequent frames using the Kanade-Lucas-Tomasi (KLT) algorithm for feature tracking [49]. To initialize the tracking process, salient points in each ROI were identified using the Harris algorithm [50]. The KLT algorithm using Harris features is known to work particularly well for tracking objects that do not change shape and for those that exhibit a rich visual texture. Hence, the KLT point tracker is often used for short-term tracking. To permit region tracking using the KLT algorithm over the full duration of each recording session, tracking videos were generated.

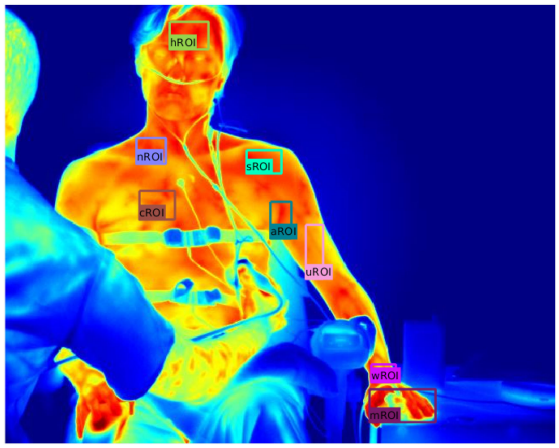

Fig. 4. Regions of interest in a sample frame of a study volunteer (29 years; 72.0 kg, 170 cm, BMI 24.9 kg/m^2). The temperature map is displayed as a heatmap. Red tones indicate higher temperatures. The ultrasound sonographer is visible on the left side. A hygro-thermometer can be seen on the table to the right.

TABLE I
BASELINE CHARACTERISTICS OF THE STUDY POPULATION

	Age (years)	Weight (kg)	Height (cm)	BMI (kg/m^2)	VLS
1	29	72.0	170	24.9	11
2	38	83.9	181	25.2	14
3	27	72.6	168	25.7	24
4	22	84.8	200	21.2	9
5	31	80.3	181	24.5	9
6	23	80.0	180	24.7	8
7	31	79.6	173	26.6	11
8	30	70.0	177	22.3	9
9	32	89.0	183	26.6	11
10	36	83.0	173	27.7	11
11	34	84.0	175	27.4	11
12	24	74.6	190	20.7	10
13	24	84.0	182	25.4	10
14	31	88.0	182	26.6	10
15	38	92.5	183	27.6	14
-	**30.0 ± 5.2**†	**81.2 ± 6.5**†	**179.9 ± 8.0**†	**25.1 ± 2.2**†	-

†Values expressed in Mean (± SD) and computed for each characteristic.
BMI = Body mass index, VLS = Von Luschan's chromatic scale [51].

To generate tracking videos from the recorded videos, we substituted frames acquired during periods of large subject motion to avoid instances of non-convergence of the KLT algorithm. A straightforward method to detect the presence this artefact is to monitor the high-frequency content in raw pixel intensities. For expediency, the sum of pixel-wise frame differences between consecutive frames was computed. Frames for which this quantity was above 2 standard deviations of its median value over all recording time (15 sessions) were substituted by the last previous frame for which this condition was not met. The KLT algorithm was used to track the position and shape of the ROIs on the generated tracking videos. In the event of non-convergence for a given frame, any *dropped* ROIs were manually reassigned for that frame, the new feature points detected (using the Harris algorithm), and frame tracking was resumed.

4) Temperature Measurements: The cutaneous temperature T_c of each thermal area was computed as the mean temperature over 25% of the pixels with the highest value of T_{obj} in that ROI (*i.e.* in the 75% percentile). The motivation for this approach is the following. Spatial T_{obj} averages computed over *all* the pixels in each ROI would be affected by the (lower temperature) values of pixels in the background for the ROI in the extremities, *e.g.* left hand, left shoulder, *etc*. Our approach avoids these confounding edge effects. To remove outliers, the resulting temperature traces were median-filtered with a filter size of 5 frames.

III. STATISTICAL ANALYSIS

Prior to statistical analysis, signals collected by the different instruments were time-aligned in the manner described in the technical note provided with this submission. The mean temperature of each thermal area during the 15-minute rest period was subtracted from the skin temperatures T_c for their respective ROI to obtain ΔT. Minute-averaged values of ΔT were computed for the two periods of interest. The changes in SV, CO, and PP were expressed as a ratio over their baseline (pre-test) values, although their absolute values were used for statistical analysis. All continuous variables were assessed for normality using the Shapiro-Wilk Test. Paired Student's t-tests were used to test for differences between pre-test values and post-values (at every minute over each period of interest) calculated as differences to theor average pre-test values to remove any influence of intersubject differences in the resting values of the physiological and thermographic variables. p-values < 0.01 were considered to be statistically significant. The statistical analysis was performed using MATLAB R2019a (MathWorks, Natick, Massachusetts, USA) and the version-compatible Statistics and Machine Learning Toolbox.

IV. RESULTS

Fifteen male, young (30 ± 5.2 years old), non-obese (body mass index (BMI): 25.1 ± 2.2 kg/m^2) adults who were not on medication and who had no history of cardiovascular disease were selected to participate in the study. Their baseline characteristics are summarised in Table I.

Fig. 5 illustrates the typical response to the two haemodynamic challenges (ET and CPT) quantified in terms of the physiological variables and surface temperature profiles for a sample experimental session. Body surface temperature was measured by infrared thermography, while the dynamics of the central and peripheral blood flow were monitored by transthoracic impedance (TTI), electrocardiography (ECG) and fingertip plethysmography (PPG). Blood pressure (BP) was measured at one-minute intervals using a brachial cuff applied to the right arm. Thermal readings during ET are omitted due to motion-induced noise in these measurements. Echographic measurements were also paused during ET.

Two periods of interest during the experiment were selected for statistical analysis: (i) the 10 minutes immediately following the cessation of ET, (ii) the 10 minutes following the start of CPT. The test-induced changes were defined as their post-test values

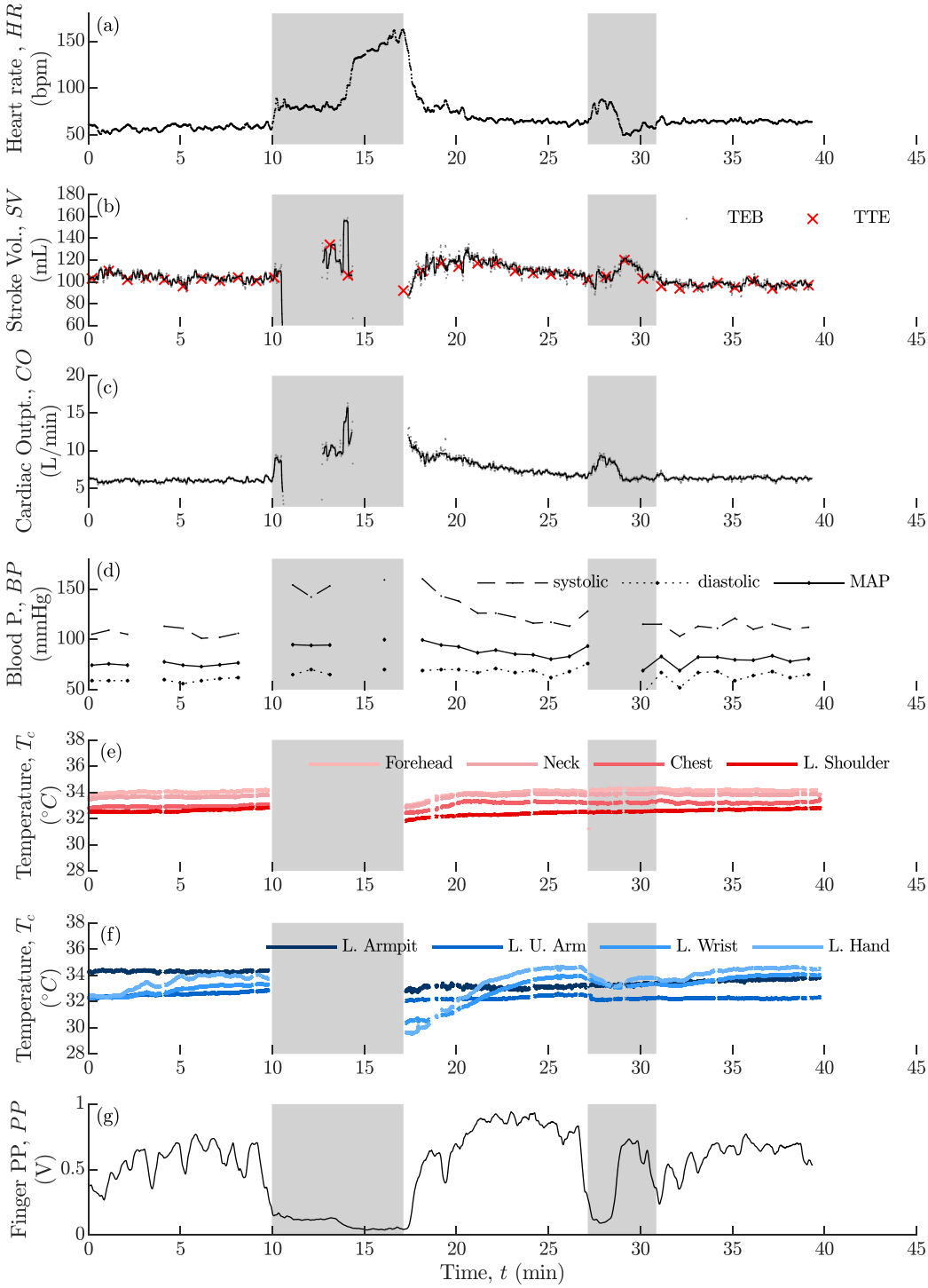

Fig. 5. Physiological response to the exercise and cold challenges in a healthy subject (24 years; 74.6 kg, 190 cm, BMI 20.7 kg/m^2): (a) heart rate, (b) stroke volume, (c) cardiac output, (d) blood pressure, average skin temperature over (e) central regions, and (f) peripheral regions, and (g) pulse pressure at the left index finger. Test periods are represented as grey-shaded areas.

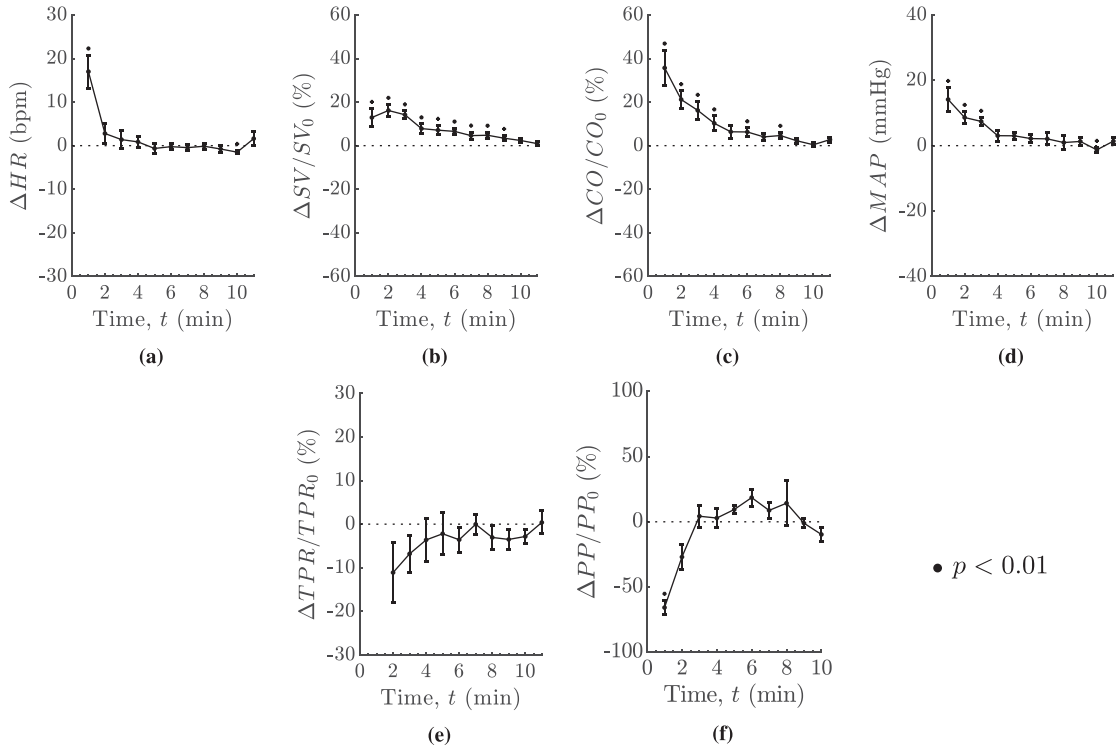

Fig. 6. Cardiovascular responses to the exercise test: (a) HR, (b) SV, (c) CO, (d) MAP, and (e) TPR, and (e) PP at the left index finger in the post-exercise recovery period. Error bars indicate the standard deviation of the sampling distributions. The changes in SV, CO, TPR, and PP are expressed as a ratio over their baseline (pre-exercise) values, although their absolute values were used for statistical analysis.

(averaged at one-minute intervals) minus their pre-test values (averaged over the 3 minutes preceding the start of each test). The paired t-test was used to compare variables in the pre-and post-test periods. Our results are presented below for the two periods of interest defined.

A. Exercise Stimulus

Exercise is associated with large haemodynamic changes involving relative redistribution of blood flow to the vascular beds of skin and muscle in the exercising and non-exercising limbs. Most cardiovascular variables were elevated following the exercise test (Fig. 6). Stroke volume (SV), cardiac output (CO), heart rate (HR), and (mean arterial pressure) MAP were significantly elevated one minute after the completion of the exercise test ($p < 0.01$). The maximal increase in HR (17.0 ± 3.8 bpm), CO ($35.7\pm$ 27.1%) and MAP ($14.1\pm$ 3.7%) occurred at $t = 1$ min while the maximal increase in SV ($16.1\pm$ 2.8%) was registered at $t = 2$ min. The significant increase in SV and CO remained for $6 - 8$ minutes after the completion of the exercise test, while on average HR returned to its baseline (pre-test) value within $1 - 2$ minutes after the start of the post-exercise recovery period. A significant elevation in MAP was sustained up to 4 minutes after ET. PPG-derived pulse pressure (PP) measured at the left index finger was used as a proxy for blood flow changes in the peripheral artery given the strong correlation between the PP signal in the fingertip and cutaneous blood flow [52]–[54]. PP registered a decrease of $61.9 \pm 6.3\%$ at the end of the exercise test. After rapid recovery period ($1 - 2$ minutes), no significant differences were measured in relation to its pre-test value.

There were significant differences in skin temperature distribution after the exercise test. Fig. 6 shows the average skin temperature data recorded in the 15 participants in the post-exercise recovery period. A significant decline in T_c following ET was seen in three peripheral thermal areas: the left upper arm (anterior view: -0.35 ± 0.13 °C at $t = 1$ min into the recovery phase), the left wrist (-1.54 ± 0.26 °C at $t = 2$ min) and the left hand (-2.09 ± 0.41 °C at $t = 1$ min). The temperature of these areas increased gradually during the post-exercise recovery period. By $t = 10$ min, no significant temperature difference was registered in relation to the pre-test period for any skin region.

A different thermal response was seen in most of the thermal areas considered as no significant temperature differences in T_c were registered in relation to their pre-exercise values. The exceptions were the forehead, neck and chest, which saw significant sub-degree temperature differences. Lower temperatures over the left shoulder ($t \leqslant 6$ min) were also observed although this decline did not reach statistical significance. These results can partly be explained by the high number of active sweat glands in the region, whose activation during ET could be easily visualised through IR imaging by the appearance of cold dots over the forehead and chest. We noted that while prior to exercise the temperature distribution over the chest and the anterior view of the neck was relatively homogeneous, during exercise the

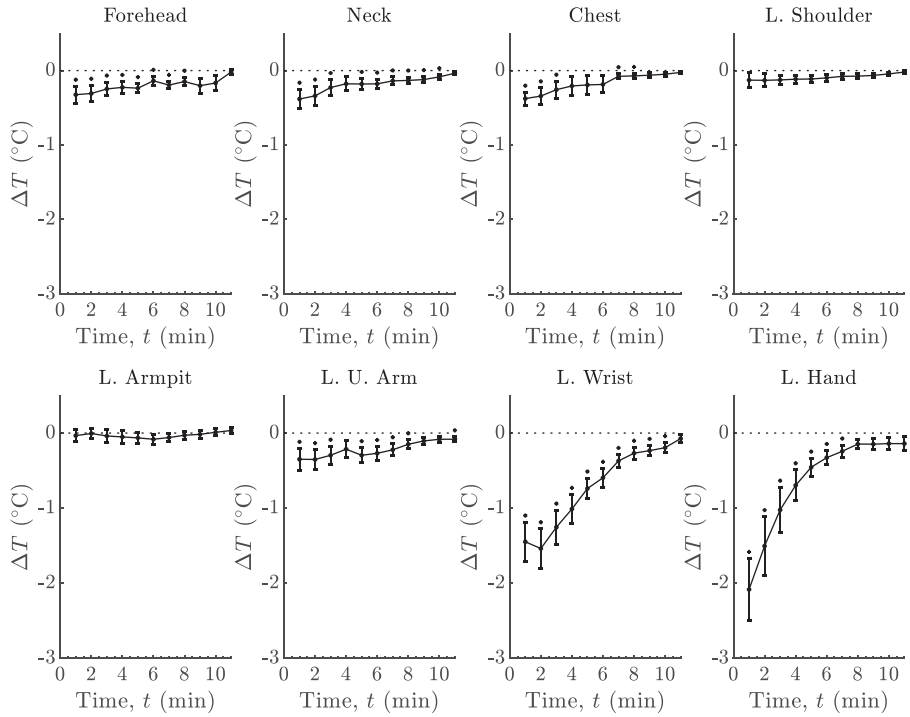

Fig. 7. Surface temperature over the 8 thermal areas at one-minute intervals following the exercise test ($t = 0$). The error bars indicate the standard deviation of the sampling distributions. $p < 0.01$.

distribution over these regions became island-shaped with dots of low radiance as a result of sweat gland activity and evaporation from the skin surface [12], [55].

B. Cold Stimulus

The median duration of the cold test was of 4.8 ± 1.3 min. The bar diagrams in Fig. 8 show the effect of this test on the cardiovascular variables. The CPT is a natural vasoconstrictor stimulus and its response is characterised by elevated MAP during the initial period of the cold stimulus (0 − 30 s) [56]. TPR increased from the control value by 14.5 ± 4.3% within 120 s of hand immersion in cold water ($p \leqslant 0.01$). MAP increased from the control value by 18.3 ± 3.4 mmHg at 60 s of immersion ($p \leqslant 0.01$), whereas the amplitude of PP declined by 70.8 ± 6.9%. HR increased from the control value by 8.1 ± 7.9 bpm at 60 s. No significant trends were observed in stroke volume or cardiac output during cold-water immersion.

The skin temperature response as a function of time is depicted in Fig. 9. Of the thermal areas recorded, the most significant reductions in T_c were recorded in the contraleral hand (−0.58 ± 0.14 °C at 180 s of immersion), and wrist (−0.42 ± 0.15 °C at 120 s of immersion). The reductions were initiated with hand immersion and resolved within 10 minutes after the start of the cold exposure. Although a mild elevation in the skin temperature over the neck region was observed, a sign test showed that there was no statistically significant temperature difference between the T_c extracted by the algorithm prior to the test and during cold-water immersion for any of the central thermal regions at the considered significance level. These results confirm that T_c exhibits variable patterns due to the redirection of cutaneous blood flow from peripheral ROIs.

C. Tracking of Thermal Regions

For generating the tracking videos, frames were substituted due to excessive motion for an average of 13.3 ± 3.7 min of recording time per volunteer session. For reference, this figure is marginally higher than the total duration of ET (10 min), the main period of subject activity in the experimental protocol. To evaluate the performance of the tracking method, we recorded the number of instances for which at least one of the 8 thermal regions was manually reassigned, *i.e.* when the convergence conditions of the Kanade-Lucas-Tomasi algorithm (usually based on error and step size) were not met. On average, this occurred for 6.8 ± 3.9 frames per volunteer session. The tracking results show that the proposed method is efficient in tracking the skin areas of interest in thermal infrared video during CPT and following ET.

V. Discussion

The principal finding of the present investigation was an association amongst perfusion changes of the vascular bed in the upper extremities and local T_c following the two haemodynamic challenges. T_c differences as a result of incremental leg exercise and a cold pressor test were measured in normal subjects using infrared thermography and analysed using appropriate statistical tests.

Physical exercise generates temperature gradients between exercising and non-exercising limbs. We found significant

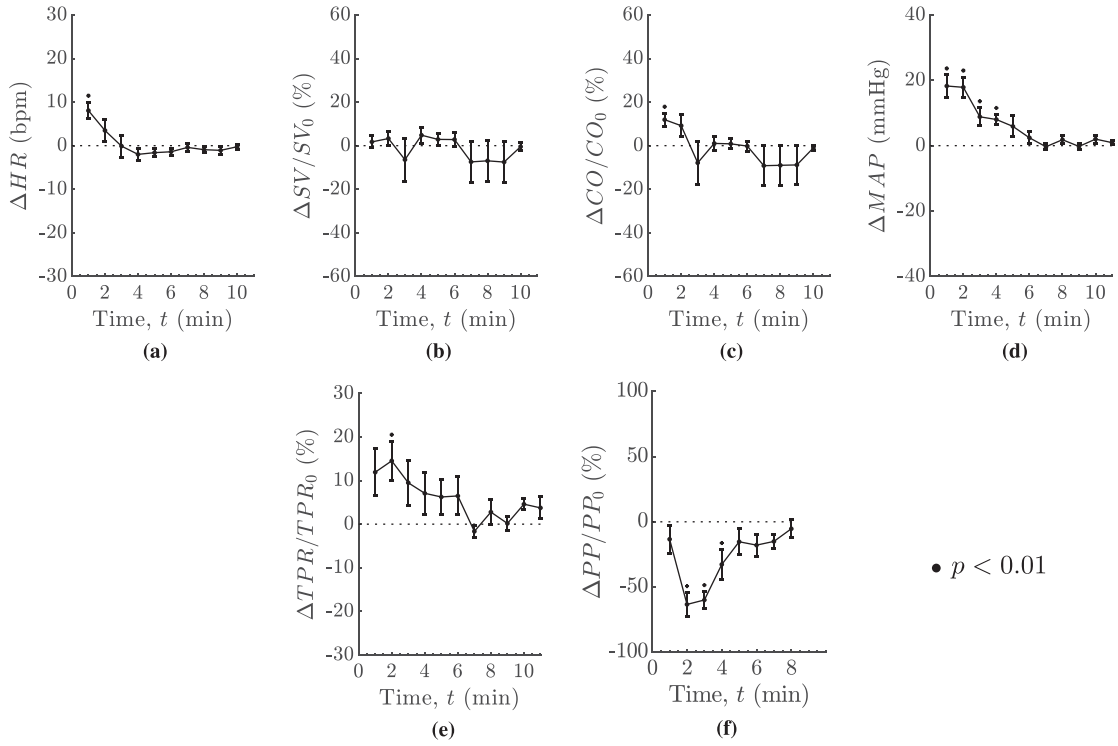

Fig. 8. Cardiovascular responses to the cold pressor test: (a) HR, (b) SV, (c) CO, (d) MAP, (e) TPR, and (e) PP at the left index finger after the start of hand immersion at $t = 0$. Error bars indicate the standard deviation of the sampling distributions. The changes in SV, CO, TPR, and PP are expressed as a ratio over their baseline (pre-CPT) values, although their absolute values were used for statistical analysis.

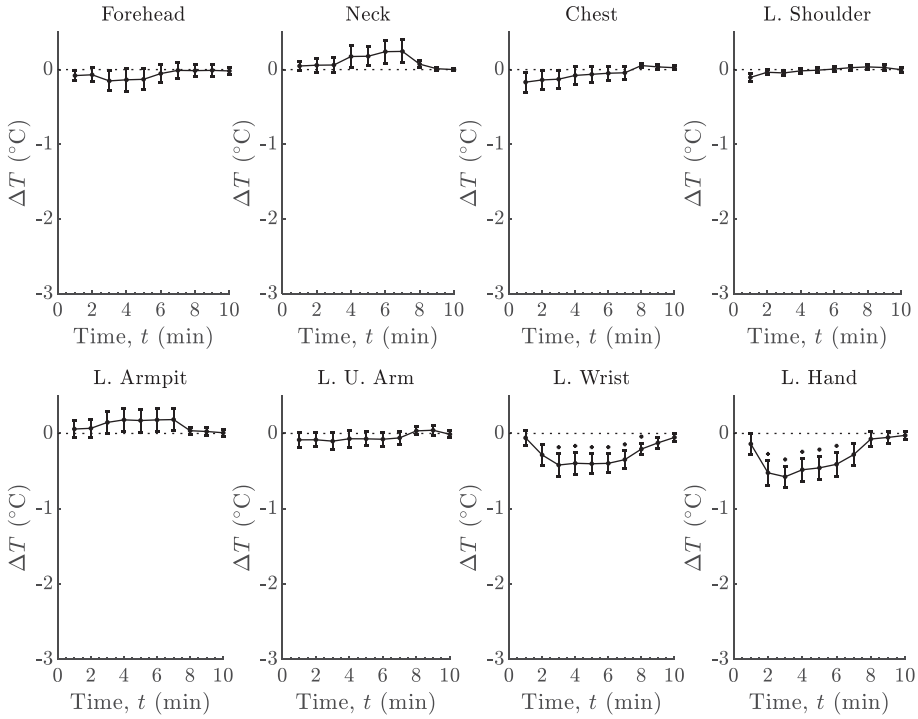

Fig. 9. Surface temperature over the 8 thermal areas at one-minute intervals following the start of the cold pressor test ($t = 0$). The error bars indicate the standard deviation of the sampling distributions. $p < 0.01$.

differences in the radiated heat distribution over the body surface of volunteers who performed 10 min of leg exercise. T_c over the non-exercising extremities (left wrist, and left hand) was significantly lowered by $1 - 2$ °C compared to pre-exercise values, while smaller (below 0.5 °C) or non-significant regional changes were found in central skin areas in the trunk and head. This peripheral cooling was accompanied by a reduction of BF to the left finger determined plethysmographically. Substantial circulatory changes occur during muscular exercise. The local thermal stimuli modulating the thermoregulatory responses during exercise are different in exercising and non-exercising limbs as the increased metabolic rate in contracting skeletal muscle increases local heat production. Additionally, BF is directed towards areas of high metabolic demand. Active muscle groups require an increased oxygen supply, which is accomplished through vasodilatation, while vasoconstriction occurs in the inactive muscle groups [57], [58].

Although the overall response, involving both thermal control and exercise, has not been thoroughly characterised, there have been numerous observations that support the notion that vasoconstrictor adjustments to exercise indeed affect the cutaneous circulation in non-exercising extremities. Christensen *et al.*, have demonstrated a rapid decrease in BF in the finger with the onset of leg exercise [59]. This decrease did not persist for longer than several minutes unless the work was very strenuous. Muth *et al.* noted a reduction in subcutaneous BF in the resting arm during supine leg exercise, which reversed with continued strenuous work [60]. Zelis *et al.*, observed that during moderate and strenuous activity forearm BF was significantly reduced in a sample of 12 healthy male subjects (ages 19 to 36 years) and 9 patients with congestive heart failure (ages 28 to 44) [61]. The latter two studies noted that a transient reduction in BF was followed by cutaneous hyperemia with continued work [60] or when exercise was discontinued [61].

A reduction in peripheral T_c immediately after exercise has also been reported [55], [57], [62]–[64]. Zontak *et al.*, reported a decrease in hand temperature in a sample of volunteers (10 male; 25.5 ± 0.7 years) exposed to constant-load and graded leg exercise [64]. The rate of temperature decrease was dependent on the initial hand temperature. Merla *et al.* and Fernandes *et al.* used thermal imaging to study whole body thermoregulation in runners during graded exercise (15 males; 25.2 ± 3.1 years [57] and 12 active males; 22.4 ± 3.3 years [55]). At the exercise interruption, Merla *et al.*, measured an average T_c difference of $3 - 5$ °C with respect to baseline across several ROIs (including the periphery). Fernandes *et al.*, noted that the most significant temperature decreases occurred in the hands (posterior view: 2.5 °C; 7.9% and anterior view: 2.4 °C; 7.7%), followed by the forearms. This is consistent with our observation that these areas elicit the greatest cutaneous response.

The CPT stimulus involves cold and pain components, and so it induces both a thermoregulatory reflex and global sympathetic activation [56]. In response to this stress, several physiological responses are triggered, which include vasoconstriction and MAP elevation, as may be confirmed from the analysis of Figures 8(e) and 8(d). The CPT was applied here to investigate the effect of reduced BF (as a result of vasoconstricted periphery) on T_c. We observed that as the right hand was immersed in ice-water, T_c in the contralateral hand and wrist significantly decreased in agreement with previous studies, which measured an average decrease in T_c between 0.5 and 1.5 °C on the contralateral hand ($p < 0.05$; 8 males and 8 females; age 21 $\pm$ 1 years) [65]. T_c in the left upper arm was also lowered during CPT, however, the temperature difference did not reach statistical significance.

In both test scenarios, the decrease in T_c in the left upper limb mirrored the decrease in BF (measured as relative changes in PP amplitude at the fingertip). This confirms our hypothesis that the relative distribution of BF to the vascular beds of skin and muscle may be monitored non-invasively through the measurement of T_c using a thermal camera. Furthermore, the magnitude of ΔT in these thermal regions was indicative of the magnitude of the reduction in PP in the left finger, *e.g.* a lower decline in T_c in the left hand as a result of CPT in comparison to the decline in T_c observed as a result of ET (-0.58 ± 0.14 °C *versus* -2.09 ± 0.41 °C) was also associated with a lower decrease in $\Delta PP/P_0$ ($-63.4 \pm 9.1\%$ *versus* $65.7 \pm 5.5\%$, although for the latter the difference is within the standard deviation for this variable). We note that the changes in T_c were independent of TPR as this variable was either decreased following ET (Fig. 6(e)) or increased with CPT (Fig. 8(e)).

Few studies have examined the dynamics of blood flow and temperature at the skin surface [12], [66]. The cold stress test showed that the decrease in T_c that occurs is slower than the associated changes in BF (see *e.g.* the T_c and PP responses to the CPT in Fig. 5 or compare the time shifts between their minima in Figures 8(f) and 9). The same effects have been observed both *in vivo* [68], [67] and in simulations [68], [69], which showed a time delay of 180 s in BF-related T_c changes. Considering the heat transfer from the vascular bed towards the skin surface as a wave process, recent modelling work established theoretical relationships for the frequency dependence of the phase delay and amplitude attenuation in T_c with respect to BF over the endothelial and neurogenic frequency bands [12]. Results of this analysis showed that the phase delay of temperature oscillations decreases with increasing frequency of BF oscillation f, as this phase delay is inversely proportional to $f^{1/2}$. This relationship may clarify the observed time delay.

Some limitations should be noted. First, clinical standard SV measurements require a transthoracic echocardiogram performed by an ultrasound radiographer. As the presence of the radiographer partially occluded the right peripheral regions (upper arm, forearm, wrist, and hand), the thermographic measurement of temperature changes over these regions could not be delivered throughout the periods of interest. As a result, a comparison between ipsilateral and contralateral responses to the cold exposure could not be attempted. Second, during the exercise test, the measurement of SV using a transthoracic biomepedance monitor, and of temperature changes using the IR thermal camera, was impaired by subject movement. As a result, we were unable to assess cardiovascular or thermal changes during this period. Future studies will explore alternative methods of inducing such changes in peripheral BF, *e.g.* in response to pharmacologically-induced haemodynamic changes, so that

physiological monitoring is not compromised (see ISRCTN study reference [70]). Finally, the tests described were performed on a small sample of healthy males. Although the volunteer study was effective in demonstrating the methodology described herein, a larger trial of patients with symptomatic peripheral vascular disease needs be conducted in order to assert whether the haemodynamics of the peripheral artery can be assessed in this population using IR thermography, *i.e.* Are the acute changes in peripheral T_c observed as a result of peripheral vasconstriction/vasodilation a good experimental proxy for changes in T_c that result from impaired BF in peripheral vessels affected by atherosclerotic disease? Are thermographic measurements over the clinically relevant anatomical regions (*e.g.* in the lower limbs) similarly feasible?

Several clinical and research applications of IR thermography require the extraction of temperature data from specific anatomical regions. Most studies in the field require specialists to manually extract these areas using manual demarcation tools. In this work, we developed a spatial tracking algorithm in order to measure continuous changes in body temperature over 8 thermal regions. Future studies on the topic of thermal patterns in humans would benefit from such automated techniques to allow for the processing of large volumes of thermographic data in a practical and reproducible manner.

VI. Conclusion

Skin perfusion is an important tool for the assessment of cardiovascular state. The present study has shown that the camera-based monitoring of the skin thermal response is feasible. The application of effective algorithms for IR image analysis is important. Further research will be directed towards the thermographic study of patients with symptomatic peripheral vascular disease.

References

[1] W. T. Meijer *et al.*, "Peripheral arterial disease in the elderly: The rotterdam study," *Arteriosclerosis, Thrombosis, Vascular Biol.*, vol. 18, no. 2, pp. 185–192, 1998.

[2] W. S. Aronow and C. Ahn, "Prevalence of coexistence of coronary artery disease, peripheral arterial disease, and atherothrombotic brain infarction in men and womenover 62 years of age," *Amer. J. Cardiol.*, vol. 74, no. 1, pp. 64–65, 1994.

[3] R. L. Morley *et al.*, "Peripheral artery disease," *BMJ*, vol. 360, 2018.

[4] F. Fowkes *et al.*, "Edinburgh artery study: Prevalence of asymptomatic and symptomatic peripheral arterial disease in the general population," *Int. J. Epidemiol.*, vol. 20, no. 2, pp. 384–392, 1991.

[5] L. Norgren *et al.*, "Inter-society consensus for the management of peripheral arterial disease (TASC II)," *J. Vascular Surgery*, vol. 45, no. 1, pp. S5–S67, 2007.

[6] K. Ouriel, "Peripheral arterial disease," *Lancet*, vol. 358, no. 9289, pp. 1257–1264, 2001.

[7] K. McLellan *et al.*, "The effects of skin moisture and subcutaneous fat thickness on the ability of the skin to dissipate heat in young and old subjects, with and without diabetes, at three environmental room temperatures," *Med. Eng. Phys.*, vol. 31, no. 2, pp. 165–172, 2009.

[8] J. S. Petrofsky *et al.*, "Skin heat dissipation: The influence of diabetes, skin thickness, and subcutaneous fat thickness," *Diabetes Technol. Therapeutics*, vol. 10, no. 6, pp. 487–493, 2008.

[9] S. Bagavathiappan *et al.*, "Infrared thermal imaging for detection of peripheral vascular disorders," *J. Med. Phys.*, vol. 34, no. 1, pp. 43–47, 2009.

[10] E. Salerud *et al.*, "Rhythmical variations in human skin blood flow," *Int. J. Microcirculation, Clin. Exp.*, vol. 2, no. 2, pp. 91–102, 1983.

[11] M. J. Geyer *et al.*, "Using wavelet analysis to characterize the thermoregulatory mechanisms of sacral skin blood flow," *J. Rehabil. Res. Develop.*, vol. 41, no. 6, pp. 797–806, 2004.

[12] A. Sagaidachnyi *et al.*, "Determination of the amplitude and phase relationships between oscillations in skin temperature and photoplethysmography-measured blood flow in fingertips," *Physiological Meas.*, vol. 35, no. 2, pp. 153–166, 2014.

[13] J. Steketee, "Spectral emissivity of skin and pericardium," *Phys. Medicine Biol.*, vol. 18, no. 5, pp. 686–694, 1973.

[14] J. Gauci *et al.*, "Automated region extraction from thermal images for peripheral vascular disease monitoring," *J. Healthcare Eng.*, vol. 2018, 2018.

[15] R. Gade and T. B. Moeslund, "Thermal cameras and applications: A survey," *Mach. Vision Appl.*, vol. 25, no. 1, pp. 245–262, 2014.

[16] "FLIR ONE Pro-Series specifications sheet (October 2019)," 2019. [Online]. Available: https://flir.netx.net/file/asset/14770/original

[17] E. Ring *et al.*, "New standards for fever screening with thermal imaging systems," *J. Mechanics Medicine Biol.*, vol. 13, no. 2, pp. 5-1–5-11, 2013.

[18] B. F. Jones and P. Plassmann, "Digital infrared thermal imaging of human skin," *IEEE Eng. Medicine Biol. Mag.*, vol. 21, no. 6, pp. 41–48, Nov.–Dec. 2002.

[19] E. F. J. Ring and K. Ammer, "The technique of infrared imaging in medicine*," in *Infrared Imaging* (2053–2563), IOP Publishing, 2015, pp. 1–10.

[20] B. Lahiri *et al.*, "Medical applications of infrared thermography: A review," *Infrared Phys. Technol.*, vol. 55, no. 4, pp. 221–235, 2012.

[21] S. J. Spalding *et al.*, "Three-dimensional and thermal surface imaging produces reliable measures of joint shape and temperature: A potential tool for quantifying arthritis," *Arthritis Res. Therapy*, vol. 10, no. 1, 2008.

[22] G. Varju *et al.*, "Assessment of hand osteoarthritis: Correlation between thermographic and radiographic methods," *Rheumatology*, vol. 43, no. 7, pp. 915–919, 2004.

[23] C. Hildebrandt and C. Raschner, "An intra-examiner reliability study of knee temperature patterns with medical infrared thermal imaging," *Thermol. Int.*, vol. 19, pp. 73–77, 2009.

[24] C. Hildebrandt *et al.*, "The application of medical infrared thermography in sports medicine," in *Proc. Ultrasound*, Feb. 2012, vol. 10, pp. 257–274.

[25] K. Ammer, "Thermal imaging: A diagnostic aid for fibromyalgia?" *Thermology Int.*, vol. 18, no. 2, pp. 45–50, 2008.

[26] M. Fischer, "Temperature and pressure threshold measurements in trigger points," *Thermology*, vol. 1, no. 4, pp. 212–215, 1986.

[27] A. Menachem, O. Kaplan, and S. Dekel, "Levator scapulae syndrome: An anatomic-clinical study," *Bulletin (Hospital Joint Diseases (New York, NY))*, vol. 53, no. 1, pp. 21–24, 1993.

[28] A. Herrick *et al.*, "Abnormal thermoregulatory responses in patients with reflex sympathetic dystrophy syndrome," *J. Rheumatol.*, vol. 21, no. 7, pp. 1319–1324, 1994.

[29] C. McCabe *et al.*, "A controlled pilot study of the utility of mirror visual feedback in the treatment of complex regional pain syndrome (type 1)," *Rheumatology*, vol. 42, no. 1, pp. 97–101, 2003.

[30] Y. Zhang *et al.*, "Attenuated skin blood flow response to nociceptive stimulation of latent myofascial trigger points," *Archives Physical Medicine Rehabilit.*, vol. 90, pp. 325–32, 2009.

[31] W. Chiu *et al.*, "Infrared thermography to mass-screen suspected sars patients with fever," *Asia Pacific J. Public Health*, vol. 17, no. 1, pp. 26–28, 2005.

[32] S. Clark *et al.*, "Comparison of thermography and laser doppler imaging in the assessment of raynaud's phenomenon," *Microvascular Res.*, vol. 66, no. 1, pp. 73–76, 2003.

[33] K. Ammer, "Cold challenge to provoke a vasospastic reaction in fingers determined by temperature measurements: A systematic review," *Thermol. Int.*, vol. 19, no. 4, pp. 109–118, 2009.

[34] M. Etehadtavakol and E. Y. Ng, "Assessment of foot complications in diabetic patients using thermography: A review," in *Application of Infrared to Biomedical Sciences*. Berlin, Germany: Springer, 2017, pp. 33–43.

[35] J. Keyserlingk *et al.*, "Functional infrared imaging of the breast: Historical perspectives, current application and future considerations," *IEEE Eng. Medicine Biol.*, vol. 19, no. 3, pp. 30–41, May/Jun. 2000.

[36] C. Herman and M. P. Cetingul, "Quantitative visualization and detection of skin cancer using dynamic thermal imaging," *J. Visualized Exp.*, no. 51, 2011, Art. no. e2679.

[37] G. Maillard and C. Hessler, "La thermographie des mélanomes malins," *Dermatology*, vol. 139, no. 5, pp. 353–358, 1969.
[38] J. Francis, R. Roggli, and T. Love, "Thermography as a means of blood perfusion measurement," *Trans. Amer. Soc. Med. Eng.*, vol. 101, no. 4, pp. 246–249, 1979.
[39] I. Pavlidis and J. Levine, "Thermal image analysis for polygraph testing," *IEEE Eng. Medicine Biol.*, vol. 21, no. 6, pp. 56–64, Nov.–Dec. 2002.
[40] I. Pavlidis *et al.*, "Interacting with human physiology," *Comput. Vision Image Understanding*, vol. 108, no. 1-2, pp. 150–170, 2007.
[41] C. Boué *et al.*, "Thermal imaging of a vein of the forearm: Analysis and thermal modelling," *Infrared Phys. Technol.*, vol. 51, no. 1, pp. 13–20, 2007.
[42] C. Jin *et al.*, "A feasible method for measuring the blood flow velocity in superficial artery based on the laser induced dynamic thermography," *Infrared Phys. Technol.*, vol. 55, no. 6, pp. 462–468, 2012.
[43] R. C. Sibley III *et al.*, "Noninvasive physiologic vascular studies: A guide to diagnosing peripheral arterial disease," *RadioGraphics*, vol. 37, no. 1, pp. 346–357, 2016.
[44] C.-L. Huang *et al.*, "The application of infrared thermography in evaluation of patients at high risk for lower extremity peripheral arterial disease," *J. Vascular Surgery*, vol. 54, no. 4, pp. 1074–1080, 2011.
[45] "Thermography guidelines. Standards and protocols in clinical thermographic imaging (September 2002)," 2002. [Online]. Available: http://www.iact-org.org/professionals/thermog-guidelines.html
[46] E. A. Hines, "A standard stimulus for measuring vasomotor reactions: Its application in the study of hypertension," *Mayo Clinic Proc.*, vol. 7, pp. 332–335, 1932.
[47] M. Harford *et al.*, "Non-invasive stroke volume estimation by transthoracic electrical bioimpedance versus doppler echocardiography in healthy volunteers," *J. Med. Eng. Technol.*, vol. 43, no. 1, pp. 33–37, 2019.
[48] FLIR, "User's manual FLIR T6xx series," *FLIR Syst.*, 2008.
[49] B. D. Lucas and T. Kanade, "An iterative image registration technique with an application to stereo vision," in *Proc. Int. Joint Conf. Artif. Intell.*, 1981, pp. 121–130.
[50] C. G. Harris *et al.*, "A combined corner and edge detector," in *Proc. Alvey Vision Conf.*, 1988, vol. 15, pp. 147–152.
[51] N. G. Jablonski, "The evolution of human skin and skin color," *Annu. Rev. Anthropol.*, vol. 33, no. 1, pp. 585–623, 2004.
[52] A. Challoner and C. Ramsay, "A photoelectric plethysmograph for the measurement of cutaneous blood flow," *Phys. Medicine Biol.*, vol. 19, no. 3, pp. 317–328, 1974.
[53] A. B. Hertzman, "The blood supply of various skin areas as estimated by the photoelectric plethysmograph," *Amer. J. Physiol.*, vol. 124, no. 2, pp. 328–340, 1938.
[54] J. De Trefford and K. Lafferty, "What does photoplethysmography measure?" *Med. Biol. Eng. Comput.*, vol. 22, no. 5, pp. 479–480, 1984.
[55] A. de Andrade Fernandes *et al.*, "Regional skin temperature response to moderate aerobic exercise measured by infrared thermography," *Asian J. Sports Medicine*, vol. 7, no. 1, 2016.
[56] L. Mourot, M. Bouhaddi, and J. Regnard, "Effects of the cold pressor test on cardiac autonomic control in normal subjects," *Physiological Res.*, vol. 58, no. 1, pp. 83–91, 2009.
[57] A. Merla *et al.*, "Thermal imaging of cutaneous temperature modifications in runners during graded exercise," *Ann. Biomed. Eng.*, vol. 38, no. 1, pp. 158–163, 2010.
[58] J. M. Johnson and D. L. Kellogg Jr, "Local thermal control of the human cutaneous circulation," *J. Appl. Physiol.*, vol. 109, no. 4, pp. 1229–1238, 2010.
[59] E. H. Christensen, M. Nielsen, and B. Hannisdahl, "Investigations of the circulation in the skin at the beginning of muscular work," *Acta Physiologica Scandinavica*, vol. 4, no. 2, pp. 162–170, 1942.
[60] H. Muth *et al.*, "Further studies of blood flow in the resting arm during supine leg exercise," *Clin. Sci.*, vol. 17, no. 1, pp. 799–806, 1958.
[61] R. Zelis, D. T. Mason, and E. Braunwald, "Partition of blood flow to the cutaneous and muscular beds of the forearm at rest and during leg exercise in normal subjects and in patients with heart failure," *Circulation Res.*, vol. 24, no. 6, pp. 799–806, 1969.
[62] T. Nakayama, Y. Ohnuki, and K. Kanosue, "Fall in skin temperature during exercise observed by thermography," *Japanese J. Physiol.*, vol. 31, no. 5, pp. 757–762, 1981.
[63] M. Torii *et al.*, "Fall in skin temperature of exercising man," *British J. Sports Medicine*, vol. 26, no. 1, pp. 29–32, 1992.
[64] A. Zontak *et al.*, "Dynamic thermography: Analysis of hand temperature during exercise," *Ann. Biomed. Eng.*, vol. 26, no. 6, pp. 988–993, 1998.
[65] Y. Isii *et al.*, "Ice-water hand immersion causes a reflex decrease in skin temperature in the contralateral hand," *J. Physiological Sci.*, vol. 57, pp. 241–248, 2007.
[66] V. Shusterman, K. P. Anderson, and O. Barnea, "Spontaneous skin temperature oscillations in normal human subjects," *Amer. J. Physiol.-Regulatory, Integrative Comparative Physiol.*, vol. 273, no. 3, pp. R1173–R1181, 1997.
[67] T. Bergersen, J. Hisdal, and L. Walløe, "Perfusion of the human finger during cold-induced vasodilatation," *Amer. J. Physiol.-Regulatory, Integrative Comparative Physiol.*, vol. 276, no. 3, pp. R731–R737, 1999.
[68] A. Shitzer *et al.*, "Lumped-parameter tissue temperature-blood perfusion model of a cold-stressed fingertip," *J. Appl. Physiol.*, vol. 80, no. 5, pp. 1829–1834, 1996.
[69] A. Sagaidachnyi *et al.*, "Real-time technique for conversion of skin temperature into skin blood flow: Human skin as a low-pass filter for thermal waves," *Comput. Methods Biomechanics Biomed. Eng.*, vol. 22, no. 12, pp. 1009–1019, 2019.
[70] "BioMed Central ISRCTN10417167: Optical monitoring of changes in perfusion map of lower limbs compared to traditional haemodynamic monitoring methods in response to pharmacological challenges in healthy volunteers or Mapping of Lower Limb skIn pErfusion (MOLLIE)," Jul. 17, 2019. [Online]. Available: https://www.isrctn.com/ISRCTN10417167